Acta Cryst. (1997). D53, 23–40

Determining Phases and Anomalous Scattering Models from the Multiwavelength Anomalous Diffraction of Native Protein Metal Clusters. Improved MAD Phase Error Estimates and Anomalous-Scatterer Positions

BRIAN R. CRANE AND ELIZABETH D. GETZOFF

Department of Molecular Biology, The Scripps Research Institute, La Jolla, CA 92037, USA.
E-mail: edg@scripps.edu

(Received 8 February 1996; accepted 31 May 1996)

Abstract

A strategy is presented for refining anomalous scattering models and calculating protein phases directly from the Bijvoet and dispersive differences of a macromolecular multiwavelength anomalous diffraction (MAD) experiment. This procedure, incorporated in the program *MADPHSREF*, is especially amenable for exploiting the weak perturbations to normal scattering produced by inner-shell electronic transitions of asymmetric metal and protein ligand assemblies. The protocol accounts for more than one type of anomalous scatterer, incorporates stereochemical restraints, treats the data in local scaling groups, and partly compensates for correlated errors. Approximating maximum likelihood by averaging observation variances and covariances over all values of phase considerably improved error estimation. Probabilistic rejection of aberrant observations, re-evaluated before each refinement cycle, improved refinement convergence and accuracy compared with other less flexible rejection criteria. *MADPHSREF* allows the facile combination of MAD phase information with phase information from other sources. For the sulfite reductase hemoprotein (SiRHP), relative weights for MAD and multiple isomorphous replacement (MIR) phases were determined by matching histograms of electron density. Accurate metal-cluster geometries and the associated errors in atomic positions can be determined from refinement against anomalous differences using normal scattering phases from a refined structure. When applied to MAD data collected on SiRHP, these methods confirmed the Fe_4S_4 cluster asymmetry initially observed in the refined 1.6 Å resolution structure and resulted in a MAD-phased, experimental, electron-density map that is of better quality than the combined MAD/MIR map originally used to determine the structure.

1. Introduction

Determining phases for macromolecular crystal structures from wavelength-dependent anomalous scattering amplitude variations is attractive in conceptual simplicity (Karle, 1989; Hendrickson, 1991), but is often experimentally demanding, as the observed differences are usually small relative to the normal scattering amplitudes and are subject to systematic errors resulting from differential absorption effects and crystal decomposition. Accurate high-resolution phasing is dependent on the accurate refinement of global anomalous scatterer positional parameters. An effective treatment of random and systematic errors is crucial for successful extraction of phases from incomplete data with weak signals and low redundancy. These problems are especially evident when native transition metal cofactors of a protein are exploited as anomalous scatterers. Protein metal clusters, commonly composed of first- or second-row transition metals (Fe, Ni, Mo), have accessible *K*-absorption edges that involve a relatively small number of electrons and, thus, their anomalous scattering only marginally affects the normal scattering intensities. Such cofactor assemblies are often asymmetric, composed of multiple atom types, and ligated by sulfides, which display small but potentially significant anomalous scattering at wavelengths that excite the metal *K*-electronic transitions. These factors complicated a multiwavelength anomalous diffraction (MAD) experiment on the 60 kDa *E. coli* sulfite reductase hemoprotein (SiRHP); the structure of which was eventually determined by a combination of MAD and multiple isomorphous replacement (MIR) (Crane, Bellamy & Getzoff, 1997; Crane, Siegel & Getzoff, 1995).

This MAD experiment endeavoured to determine structure-factor phases from the anomalous scattering of five native Fe atoms contained in SiRHP's cofactors: one ferric siroheme (tetrahydroporphyrin of the isobacteriochlorin class) covalently linked to one $Fe_4S_4^{2+}$ cluster by a bridging cysteine thiolate. Diffraction data collected on beamline 1-5AD of the Stanford Synchrotron Radiation Laboratory (SSRL) in 1992 were measured at three wavelengths: one at the Fe *K*-absorption edge to accentuate $\Delta f'$ [$\lambda_C = 1.7412$ Å (7120.4 eV)], one at the Fe *K*-absorption peak to accentuate $\Delta f''$ [$\lambda_B = 1.7374$ Å (7135.9 eV)], and one

at a remote wavelength [$\lambda_A = 1.5418$ Å (8041.1 eV)] to provide large dispersive differences relative to observations taken at λ_B and λ_C. The low redundancy, lack of completeness and discrepancies among redundant measurements of amplitudes made phase determination from the SiRHP MAD diffraction data a considerable challenge with the methods available at the time of the experiment (Crane *et al.*, 1997). Previous MAD experiments involving iron–sulfur containing proteins have been primarily successful at extracting low-resolution phases. For ferredoxin, MAD phases were determined to 5.0 Å resolution (Murthy, Hendrickson, Orme-Johnson, Merritt & Phizackerley, 1988), while for 5-phosphoribosyl-1-pyrophosphate (PRPP) amidotransferase, MAD phases of resolution beyond 5.5 Å had to be improved by non-crystallographic symmetry averaging (Smith *et al.*, 1994).

The development of the program *MADPHSREF* was motivated by the desire to refine accurately anomalous scatterer parameters and improve phase determination from the limited SiRHP MAD data. *MADPHSREF* refines an anomalous scattering model directly against Bijvoet and dispersive differences while making maximum likelihood estimates of errors, applying stereochemical restraints, taking into account more than one type of anomalous scatterer, probabilistically rejecting outlying observations, and partly compensating for inherent correlations between lack-of-closure expressions. Assuming fixed normal scattering phases from the refined SiRHP structure, this refinement method also allowed subtle asymmetries in the SiRHP Fe_4S_4 cluster to be characterized using the relatively weak MAD data. Anomalous dispersion effects are independent of the protein's normal scattering atoms, enabling parameters associated with the anomalous scatterers to be refined independently of all other parameters. Hence, the refinement of the anomalous model is greatly overdetermined and the least-squares normal matrix, which is much smaller than the corresponding matrix for normal scattering, can be easily inverted to obtain estimated errors. Given well measured data, this increased overdetermination should lead to more accurate protein metal-center geometries than would be obtained by a conventional normal scattering refinement.

Limitations of refining the perturbative scattering model with non-linear least-squares, where the non-perturbative structure-factor phases for normal protein scattering (φ_P's) are fixed and iteratively updated, are less severe for a MAD experiment compared with an MIR experiment. Non-linear least-squares refinement of heavy-atom parameters has long been applied to isomorphous phasing (Dickerson, Kendrew & Strandberg, 1991). In early applications to MIR, global heavy-atom parameters on which all structure factors depend (*e.g.* heavy-atom positions, occupancies and thermal factors) were refined, while parameters local to a given structure factor (*e.g.* φ_P) were held constant and then re-evaluated between refinement cycles. Because the protein phases are implicit functions of sets of global heavy-atom parameters for each derivatives, this type of refinement can become considerably biased when fixed phases attempt to reinforce the heavy-atom scattering model that has defined them. For MIR least-squares refinement, ignoring the implicit interdependence of local and global parameters leads to a block-diagonal normal refinement matrix where the residuals of one derivative are not influenced by the parameters of another, even though all derivatives are mutually dependent on the protein phase. One strong derivative, separated from the influence of the others, can severely bias the refinement and limit convergence (Blow & Matthews, 1977). Many workers have explored strategies to overcome these limitations (Dodson, 1976; Sygusch, 1977; Bricogne, 1984; Terwilliger & Eisenberg, 1987; Otwinowski, 1991), with a complete maximum likelihood refinement being the most rigorous (Bricogne, 1991). In contrast, a MAD experiment based on native anomalous scatterers involves only a single set of global parameters that all Bijvoet and dispersive difference depend upon (*i.e.* the positions, thermal factors, and occupancies of the anomalous scatterers). Hence, ignoring the implicit dependence of the protein phase on the global parameters of the perturbative scattering model is a reasonable approximation, especially if the starting atomic coordinates are close to their true values. However, this does introduce correlated errors among the residuals that arise from mutual dependence of like observations on the same anomalous scattering model, the same normal scattering model, and systematic measurement error. Compensation for these inherent correlations can considerably aid the stability and accuracy of refinement.

The absolute errors contained within a phase set determined from a specific experiment (such as MAD or MIR) may not be accurately reflected by the estimated figures of merit (FOM) for individual reflections, even though the relative error estimates within a resolution range of one specific phase set are reasonable. An independent criterion for the assessment of relative weighting schemes would be beneficial when combining phases from different sources. Proteins with similar solvent content have characteristic electron-density distributions within a specified range of resolution (Zhang & Main, 1990). For SiRHP, appropriate weighting between the MAD and MIR phases was determined by comparing electron-density histograms calculated from the MAD/MIR combined phases to electron-density histograms of known crystal structures with similar solvent content. Taken together, the phasing strategies and weighting schemes presented here and implemented in the program *MADPHSREF* resulted in a considerably improved, readily

interpretable experimental electron-density map for SiRHP.

2. Methodology

2.1. *An exact expression for anomalous scattering from one atom type*

The fundamental scattering equation for one type of anomalous scatterer can be expressed in a form that is linear in wavelength-independent terms and can be solved for these parameters by a least-squares procedure (Hendrickson, 1991; Hendrickson, Smith, Phizackerley & Merritt, 1988).

$$|F^{\pm}(\lambda)|^2 = |^{\circ}F_T|^2 + a(\lambda)|^{\circ}F_A|^2 + b(\lambda)|^{\circ}F_T||^{\circ}F_A| \times \cos(^{\circ}\varphi_T - ^{\circ}\varphi_A) \pm c(\lambda)|^{\circ}F_T||^{\circ}F_A| \times \sin(^{\circ}\varphi_T - ^{\circ}\varphi_A) \quad (1)$$

$$^{\circ}F_T = |^{\circ}F_T|\exp(i\varphi_T) \quad (2)$$

$$^{\circ}F_A = |^{\circ}F_A|\exp(i\varphi_A), \quad (3)$$

where for the wavelength-dependent terms,

$$a(\lambda) = [(f')^2 + (f'')^2]/(f^{\circ})^2 \quad (4)$$

$$b(\lambda) = 2(f'/f^{\circ}) \quad (5)$$

$$c(\lambda) = 2(f''/f^{\circ}). \quad (6)$$

$^{\circ}F_T$ represents the total scattering vector from all normal scattering in the unit cell, $^{\circ}F_A$ represents the normal scattering vector from all atoms that scatter anomalously, f° is the normal atomic scattering factor for the anomalously scattering atoms, and f' and f'' are orthogonal components of the atomic anomalous-scattering factor. This approach, implemented in the program *MADLSQ* (Hendrickson *et al.*, 1988), has proven very effective when there is one dominant type of anomalous scatterer and a system of (1) is sufficiently overdetermined for the four wavelength-independent parameters $[|^{\circ}F_T|, |^{\circ}F_A|, \cos(^{\circ}\varphi_T - ^{\circ}\varphi_A)$, and $\sin(^{\circ}\varphi_T - ^{\circ}\varphi_A)]$ by at least six or more individual observations per phase (Wu, Lustbader, Lin, Canfield & Hendrickson, 1994; Hubbard, Wei, Ellis & Hendrickson, 1994; Shapiro *et al.*, 1995). However, when the signal-to-noise ratio is weak and the number of independent observations per phase is ≤ 4, the least-squares treatment can be unstable and produce aberrant parameter estimates (Crane *et al.*, 1997).

2.2. *Anomalous scattering expressed in separate terms for Bijvoet and dispersive differences*

Another strategy for extracting normal-scattering phases from anomalous-scattering effects derives from the induced amplitude differences between Bijvoet pairs of a given reflection at a given wavelength,

$$\Delta|F^{\pm}(\lambda_i)| = |F^{+}(\lambda_i)| - |F^{-}(\lambda_i)|, \quad (7)$$

and the dispersive amplitude difference between measurements of a given reflection collected at two wavelengths,

$$\Delta|\bar{F}(\lambda_{ij})| = |\bar{F}(\lambda_i)| - |\bar{F}(\lambda_j)|, \quad (8)$$

where,

$$|\bar{F}(\lambda_i)| = [|F^{+}(\lambda_i)| + |F^{-}(\lambda_i)|]/2. \quad (9)$$

As noted by Terwilliger (Terwilliger, 1994), errors in $\Delta|\bar{F}(\lambda_{ij})|$ are unlikely to be correlated with errors in $\Delta|F^{\pm}(\lambda_i)|$ because the size of the difference between Bijvoet pairs at a given wavelength is uncorrelated to the size of their average.

Referring to Fig. 1(*a*) and assuming that the phase for the normal scattering vector (protein phase φ_P) is constant for $^{\circ}F_T$, $|\bar{F}(\lambda_i)|$ and $|\bar{F}(\lambda_j)|$,

$$|\bar{F}(\lambda_j)|^2 = |\bar{F}(\lambda_i)|^2 + |\Delta F'_A(\lambda_{ij})|^2 - 2|\bar{F}(\lambda_i)||\Delta F'_A(\lambda_{ij})|\cos(\varphi_P - \psi_D), \quad (10)$$

or,

$$\Delta|\bar{F}(\lambda_{ij})| = -\frac{|\Delta F'_A(\lambda_{ij})|^2}{|\bar{F}(\lambda_i)| + |\bar{F}(\lambda_j)|} + 2\frac{|\bar{F}(\lambda_i)||\Delta F'_A(\lambda_{ij})|}{|\bar{F}(\lambda_i)| + |\bar{F}(\lambda_j)|}\cos(\varphi_P - \psi_D), \quad (11)$$

where ψ_D is the phase for the dispersive component of the total resonance scattering vector from all atom types, and $|\Delta F'_A(\lambda_{ij})|$ is its magnitude. If we assume that $N_A^{1/2}[\Delta f'(\lambda_{ij})] \ll N_P^{1/2}(\bar{f}^{\circ})$, where $\bar{f}^{\circ}$ is the average normal scattering factor for N_P atoms in the unit cell, and N_A is the number of anomalously scattering atoms, then $|\Delta F'_A(\lambda_{ij})|$ will be small compared with $|\bar{F}(\lambda_j)|$ and φ_P will not vary much between $|\bar{F}(\lambda_i)|$ and $|\bar{F}(\lambda_j)|$; *i.e.* $|\bar{F}(\lambda_i)|$ and $|\bar{F}(\lambda_j)|$ will be approximately equal. (11) then reduces to,

$$\Delta|\bar{F}(\lambda_{ij})| \simeq |\Delta F'_A(\lambda_{ij})|\cos(\varphi_P - \psi_D), \quad (12)$$

or,

$$\Delta|\bar{F}(\lambda_{ij})| \simeq (A_D\cos\varphi_P + B_D\sin\varphi_P), \quad (13)$$

where,

$$A_D = |\Delta F'_A(\lambda_{ij})|\cos(\psi_D) \quad (14)$$

$$B_D = |\Delta F'_A(\lambda_{ij})|\sin(\psi_D). \quad (15)$$

Terms for the anomalous differences between Bijvoet pairs can be derived from the relationship shown in Fig. 1(*b*), assuming φ_P constant for $^{\circ}F_T$, $F^{+}(\lambda_i)$ and $F^{-}(\lambda_i)$,

$$|F^{+}(\lambda_i)|^2 - |\bar{F}(\lambda_i)|^2 = |F''_A(\lambda_i)|^2 - 2|\bar{F}(\lambda_i)||F''_A(\lambda_i)| \times \cos[\pi - (\psi_A - \varphi_P)], \quad (16)$$

and,

$$|F^-(\lambda_i)|^2 - |\bar{F}(\lambda_i)|^2 = |F''_A(\lambda_i)|^2 - 2|\bar{F}(\lambda_i)||F''_A(\lambda_i)| \times \cos(\varphi_P - \psi_A). \quad (17)$$

Combining (16) and (17) gives,

$$|F^+(\lambda_i)|^2 - |F^-(\lambda_i)|^2 = 4|\bar{F}(\lambda_i)||F''_A(\lambda_i)|\cos(\varphi_P - \psi_A), \quad (18)$$

where $|F''_A|$ and ψ_A are the amplitude and phase of the anomalous component of the total resonance scattering vector from all atom types. Since $|F''_A(\lambda_i)|$ is usually small compared with $|\bar{F}(\lambda_i)|$ (18) reduces (Hendrickson & Teeter, 1981) to,

$$\Delta|F^\pm(\lambda_i)| \simeq 2|F''_A(\lambda_i)|\cos(\varphi_P - \psi_A), \quad (19)$$

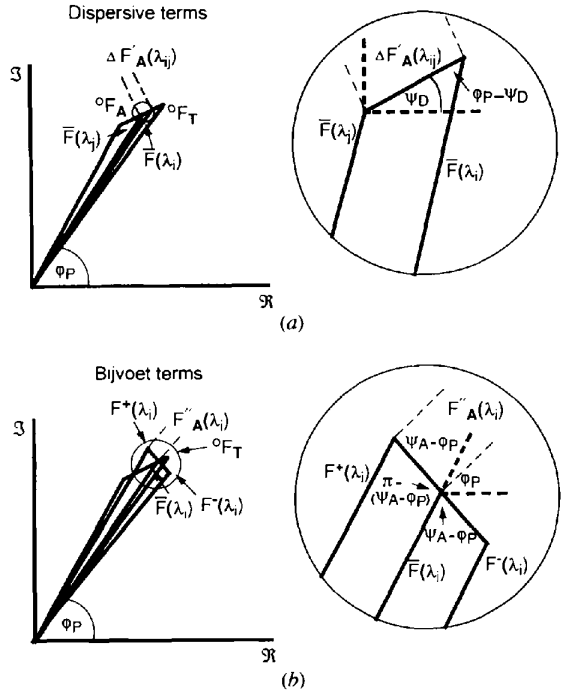

Fig. 1. Argand diagrams depicting the relationships between the normal and anomalous scattering vectors of a structure factor. (*a*) Relation of the dispersive difference between $\bar{F}(\lambda_i)$ and $\bar{F}(\lambda_j)$, $[\Delta F'_A(\lambda_{ij})]$ to the normal-scattering structure factors $^\circ F_T$ (all normal scattering) and $^\circ F_A$ (normal scattering from the atoms that also scatter anomalously). ψ_D is the phase of $\Delta F'_A(\lambda_{ij})$. (10) is derived from the law of cosines applied to the triangle with sides $\bar{F}(\lambda_j)$, $\bar{F}(\lambda_i)$, and $\Delta F'_A(\lambda_{ij})$. The normal scattering protein phase φ_P is assumed the same for $\bar{F}(\lambda_i)$, $\bar{F}(\lambda_j)$ and $^\circ F_T$ in the derivation of (12). (*b*) Relation of the Bijvoet difference between $F^+(\lambda_i)$ and $F^-(\lambda_i)$ $[F''_A(\lambda_i)]$ to the normal-scattering structure factors $^\circ F_T$ and $^\circ F_A$. (16) and (17) are derived from the law of cosines applied to the triangles with sides $F^+(\lambda_i)$, $\bar{F}(\lambda_i)$, and $\Delta F''_A(\lambda_i)$ (at left) and sides $F^-(\lambda_i)$, $\bar{F}(\lambda_i)$, and $\Delta F''_A(\lambda_i)$ (at right). Note that with more than one type of anomalous scatterer ψ_A, the phase of $F''_A(\lambda_{ij})$, need not be perpendicular to the phase of $^\circ F_A$. The normal scattering protein phase φ_P is assumed the same for $F^+(\lambda_i)$, $F^-(\lambda_i)$ and $\bar{F}(\lambda_i)$ in the derivation of (19).

or,

$$\Delta|F^\pm(\lambda_i)| \simeq 2(A_A\cos\varphi_P + B_A\sin\varphi_P), \quad (20)$$

where,

$$A_A = |F''_A(\lambda_i)|\cos(\psi_A) \quad (21)$$

$$B_A = |F''_A(\lambda_i)|\sin(\psi_A). \quad (22)$$

2.3. *Non-linear least-squares refinement, a likelihood approximation for phase probability distributions and the inherent correlation of errors*

The calculated Bijvoet and dispersive differences for a given reflection depend on the global parameters of each anomalous scatterer, the local parameter of normal scattering phase, and the local scale and thermal factors applicable to the section of reciprocal space where and when the reflection is measured.

$$\Delta|F^\pm(\lambda_i)|_{\text{calc}} = f[r_q, f''_q(\lambda_i), B_q, \text{Occ}_q, \text{Bov}_l, \text{Sc}_l, \varphi_P] = f(\varepsilon_A), \quad (23)$$

$$\Delta|\bar{F}(\lambda_{ij})|_{\text{calc}} = f[r_q, \Delta f'_q(\lambda_{ij}), B_q, \text{Occ}_q, \text{Bov}_l, \text{Sc}_l, \varphi_P] = f(\varepsilon_D), \quad (24)$$

where the set of parameters ε_{AD} contains: the coordinates of the anomalously scattering atom q, r_q; its difference anomalous scattering-factor components for λ_i and λ_j, $\Delta f'_q(\lambda_{ij})$ and $f''_q(\lambda_i)$; its thermal factors and occupancy, B_q and Occ_q; the overall scale, Sc_l, and thermal factor, Bov_l, for local scaling group l; and the normal scattering protein phase, φ_P. We can define the error functions,

$$\Delta_A(\lambda_i) = \Delta|F^\pm(\lambda_i)|_{\text{obs}} - \Delta|F^\pm(\lambda_i)|_{\text{calc}} \quad (25)$$

$$\Delta_D(\lambda_{ij}) = \Delta|\bar{F}(\lambda_{ij})|_{\text{obs}} - \Delta|\bar{F}(\lambda_{ij})|_{\text{calc}}. \quad (26)$$

The likelihood of our anomalous scattering model being correct given the observed data is then given by Bayes rule (Zehna, 1970),

$$\Lambda(\varepsilon_{AD}|\Delta_A, \Delta_D) = \prod_{\mathbf{h}} P_{\mathbf{h}}(\Delta_A|\varepsilon_{AD})\cdot P_{\mathbf{h}}(\Delta_D|\varepsilon_{AD})\cdot P^\circ_{\mathbf{h}}(\varepsilon_{AD}), \quad (27)$$

where $\mathbf{h}$ represents an individual reflection, $P_{\mathbf{h}}(\Delta_A|\varepsilon_{AD})$ and $P_{\mathbf{h}}(\Delta_D|\varepsilon_{AD})$ are the probability of observing Δ_A or Δ_D, given the parameter set ε_{AD}, and $P^\circ_{\mathbf{h}}(\varepsilon_{AD})$ is an *a priori* distribution for ε_{AD}. $P^\circ_{\mathbf{h}}(\varepsilon_{AD})$ can incorporate the expected distribution of the difference anomalous scattering vectors [which should conform to Wilson statistics (Wilson, 1949)], or information on the relative positions of the anomalously scattering atoms (which can alternatively be applied as stereochemical restraints during refinement).

To compensate for correlations between the residual errors of pairs of Bijvoet differences and between the residual errors of pairs of dispersive differences we assume multivariate Gaussian error distributions. Error

vectors for the anomalous and dispersive terms can be defined as,

$$\mathbf{\Delta_A} = \{\Delta_A(\lambda_i), \Delta_A(\lambda_j), \Delta_A(\lambda_k), \ldots\} \quad (28)$$

$$\mathbf{\Delta_D} = \{\Delta_D(\lambda_{ij}), \Delta_D(\lambda_{ik}), \Delta_D(\lambda_{jk}), \ldots\}. \quad (29)$$

Then,

$$P_{\mathbf{h}}(\mathbf{\Delta_A}|\varepsilon_A) \propto \exp[-1/2(\mathbf{\Delta_A}^T \cdot \mathbf{V_A}^{-1} \cdot \mathbf{\Delta_A})], \quad (30)$$

and,

$$P_{\mathbf{h}}(\mathbf{\Delta_D}|\varepsilon_D) \propto \exp[-1/2(\mathbf{\Delta_D}^T \cdot \mathbf{V_D}^{-1} \cdot \mathbf{\Delta_D})], \quad (31)$$

where $\mathbf{V_A}$ and $\mathbf{V_D}$ are the covariance matrices for the Bijvoet and dispersive error functions, respectively.

For a MAD experiment performed at three wavelengths,

$$\mathbf{V_A} = \begin{pmatrix} E_{11} & E_{12} & E_{13} \\ \cdot & E_{22} & E_{23} \\ \cdot & \cdot & E_{33} \end{pmatrix},$$

where the terms along the diagonal represent variances for $\Delta_A(\lambda_i), \Delta_A(\lambda_j), \Delta_A(\lambda_k)$, averaged over all reflections in a selected bin of resolution, while the off-diagonal terms represent covariances between residuals calculated from Bijvoet differences measured at different wavelengths (and likewise for the dispersive terms).

The total probability distribution for the phase of a given reflection ($P_{\mathbf{h}}^T$) is then,

$$P_{\mathbf{h}}^T = P_{\mathbf{h}}(\mathbf{\Delta_A}|\varepsilon_{AD}) \cdot P_{\mathbf{h}}(\mathbf{\Delta_D}|\varepsilon_{AD}) \cdot P_{\mathbf{h}}^{\circ}(\varepsilon_{AD}). \quad (32)$$

By integrating over all values of phase we can determine centroid values for phase,

$$\langle\varphi_P\rangle = \frac{\int_{\varphi_P} \varphi_P P_{\mathbf{h}}^T \mathrm{d}\varphi_P}{\int_{\varphi_P} P_{\mathbf{h}}^T \mathrm{d}\varphi_P}, \quad (33)$$

and for the figure of merit,

$$FOM = \left| \frac{\int_{\varphi_P} \exp(i\varphi_P) P_{\mathbf{h}}^T \mathrm{d}\varphi_P}{\int_{\varphi_P} P_{\mathbf{h}}^T \mathrm{d}\varphi_P} \right|. \quad (34)$$

Maximizing the likelihood function (27) is equivalent to minimizing its negative logarithm,

$$\sum_{\mathbf{h}} 1/2[\mathbf{\Delta_A}^T \cdot \mathbf{V_A}^{-1} \cdot \mathbf{\Delta_A}] + \sum_{\mathbf{h}} 1/2[\mathbf{\Delta_D}^T \cdot \mathbf{V_D}^{-1} \cdot \mathbf{\Delta_D}] \quad (35)$$

Although φ_P must be fixed for each refinement cycle, the propagation of errors resulting from an invariant φ_P can be limited by averaging the covariance matrix over all values of phase instead of simply evaluating errors at the centroid phase,

$$\langle E_{ij}\rangle = \frac{\int_{\varphi_P} E_{ij} P_{\mathbf{h}}^T \mathrm{d}\varphi_P}{\int_{\varphi_P} P_{\mathbf{h}}^T \mathrm{d}\varphi_P}. \quad (36)$$

This is effectively a maximum-likelihood estimate of the error matrix over the variable of phase. Maximum-likelihood estimates of error variances have been shown to provide much more accurate error estimates for MIR refinement (Terwilliger & Eisenberg, 1987; Otwinowski, 1991).

Non-linear least-squares refinement of the anomalous scattering model can be applied to minimizing (35) with intermittent recalculation of protein phases based on updated refined parameters and error estimates. Under first-order approximations, where the second-order partial derivatives of the normal matrix are approximated by products of first-order derivatives, the correlation of errors among related anomalous and dispersive differences introduces cross-over terms to the summed normal matrix elements of the type,

$$\sum_{uv} \left\{ \frac{\partial\Delta|F^{\pm}(\lambda_i)|_{\mathrm{calc}}}{\partial\varepsilon_u} \right\} \left\{ \frac{\partial\Delta|F^{\pm}(\lambda_j)|_{\mathrm{calc}}}{\partial\varepsilon_v} \right\} + \left\{ \frac{\partial\Delta|F^{\pm}(\lambda_j)|_{\mathrm{calc}}}{\partial\varepsilon_u} \right\} \left\{ \frac{\partial\Delta|F^{\pm}(\lambda_i)|_{\mathrm{calc}}}{\partial\varepsilon_v} \right\}, \quad (37)$$

where u and v denote parameters in the set of ε_{AD}. (13) and (20) separate φ_P from the global parameters, allowing first-order derivatives of the global parameters to be readily calculated,

$$\frac{\partial\Delta|\overline{F}(\lambda_{ij})|_{\mathrm{calc}}}{\partial\varepsilon_u} = \frac{\partial A_D}{\partial\varepsilon_u}\cos\varphi_P + \frac{\partial B_D}{\partial\varepsilon_u}\sin\varphi_P, \quad (38)$$

and

$$\frac{\partial\Delta|F^{\pm}(\lambda_i)|_{\mathrm{calc}}}{\partial\varepsilon_u} = 2\frac{\partial A_A}{\partial\varepsilon_u}\cos\varphi_P + 2\frac{\partial B_A}{\partial\varepsilon_u}\sin\varphi_P. \quad (39)$$

During refinement, individual reflections are weighted by their observed measurement error (σ) and the FOM calculated in the previous cycle. Geometrical restraints, representing prior structural knowledge, can be placed on any metal clusters (*e.g.* the distance restraints imposed by an iron–sulfur cluster cubane). This is equivalent to providing an *a priori* distribution $P^{\circ}(\varepsilon_{AD})$ on the scatterer positions. Refining separate overall scale and overall thermal parameters for wedges of diffraction data collected on different crystals, over different fractions of reciprocal space, or at different times can help reduce systematic experimental error. To cast MAD-derived probability distributions ($P_{\mathbf{h}}^T$) into Hendrickson–Lattman (*ABCD*) coefficients (Hendrickson & Lattman, 1970) for combination with other MAD phase distributions from symmetry-related reflections or for combination with phasing information from other sources (such as MIR), the *ABCD* exponential terms are integrated over $P_{\mathbf{h}}^T$,

$$A = \int_{\varphi_P} \cos\varphi(P_{\mathbf{h}}^T)\mathrm{d}\varphi_P \quad (40)$$

$$B = \int_{\varphi_P} \sin\varphi(P_{\mathbf{h}}^T)\mathrm{d}\varphi_P \quad (41)$$

$$C = \int_{\varphi_P} \cos 2\varphi(P_{\mathbf{h}}^T)\mathrm{d}\varphi_P \quad (42)$$

$$D = \int_{\varphi_P} \sin 2\varphi(P_{\mathbf{h}}^T)\mathrm{d}\varphi_P. \quad (43)$$

For the first cycle of phase calculation only, the covariance matrix **V** is estimated by choosing reflections with large anomalous and dispersive differences (between 2 and 4σ) and assuming ψ_A perpendicular to φ_P and ψ_D colinear with φ_P. The covariance matrix is estimated separately for centric reflections because centric reflections, owing to their restricted phases, are expected to have variances twice as large as would be found for acentric reflections (Terwilliger & Eisenberg, 1987).

2.4. *The rejection of aberrant observations*

Because the anomalous scattering signal-to-noise ratio is often small, wide variances result for the distribution of differences between observed and calculated values. Many observed differences can even have the wrong sign. When present in large numbers, these aberrant measurements severely limit the ability of the refinement to converge. Providing that the starting parameter model is close to the correct one, discrepant observations can be identified for rejection by comparing observed values with those calculated from the current model. We implemented a probabilistic rejection protocol to remove inconsistent observations without unduly biasing the refinement. An observed difference (Δ_A or Δ_D) is rejected if,

$$\mathrm{Ran} \geq \exp[-\mathrm{Ze} \cdot (\Delta_A^2/2E_A^2)], \quad (44)$$

or

$$\mathrm{Ran} \geq \exp[-\mathrm{Ze} \cdot (\Delta_D^2/2E_D^2)], \quad (45)$$

where Ran is a randomly generated number between 0 and 1, E is the current estimate of the root-mean-square error for a Bijvoet (A) or dispersive (D) difference, and Ze is an adjustable parameter that sets the rejection level. Thus, an observation that produces a large error residual compared to the present model and current E-value estimate will have a greater probability of being rejected on the current cycle. Reflections to be rejected are reselected at the beginning of each refinement cycle and all observations are always allowed to contribute to the phase distributions. In this way, observations that do not agree with the current model still have the opportunity to influence the refinement at a later stage. These selection criteria will reduce bias of the starting model but also have the potential to induce oscillatory behavior and prevent convergence.

2.5. *Full-matrix least-squares refinement of anomalous scatterer positions*

The refinement of the positions of anomalously scattering atoms against anomalous and dispersive differences can also be useful for assessing asymmetries in metal clusters. In this case, φ_P is held fixed at a value calculated from a refined structure, and full-matrix least-squares refinement can generate the covariance matrix containing estimated standard deviations in atomic parameters. Observations are scaled to the calculated model amplitudes by relative Wilson scaling and weighted by their measurement σ and Sim weight on φ_P (W) (Sim, 1959).

$$W = I_1(X)/I_0(X) \quad (46)$$

$$X = \frac{2|F_{\mathrm{obs}}||F_{\mathrm{calc}}|}{\langle|F_{\mathrm{obs}}|^2 - |F_{\mathrm{calc}}|^2\rangle}, \quad (47)$$

where I_0 and I_1 are zero and first order Bessel functions, respectively, and the denominator of X is fit to a resolution-dependent second-degree polynomial.

2.6. *Weighting MAD and MIR phase distributions by histogram matching*

MAD-derived phase probability distributions can be combined with phase probability distributions from other sources by summing Hendrickson–Lattman coefficients that represent the respective distributions. Comparisons of electron-density histograms calculated from the combined experimental phase sets to histograms derived from previously determined protein structures is an effective way to weight the coefficients. A histogram of an electron-density map is the probability distribution of the electron density at the grid points of the map. The density frequency in bin z of map M is defined as,

$$f_z^M = \frac{n_Z}{N_{\mathrm{tot}}}, \quad (48)$$

where N_{tot} is the total number of grid points and n_z is the number of grid points that have an electron density (ρ) within the range for bin z. Density values are partitioned into equally spaced bins to create the histogram,

$$\frac{-w \cdot \sigma_M}{2} + \frac{w \cdot \sigma_M}{\mathrm{nbin}}(z-1) \leq \rho < -\frac{-w \cdot \sigma_M}{2} + \frac{w \cdot \sigma_M}{\mathrm{nbin}}(z), \quad (49)$$

where σ_M is the r.m.s. value of electron-density in map M and w is the total width of the electron-density distribution in terms of σ_M. All values less than $(-w \cdot \sigma_M/2)$

Table 1. *Data and refinement statistics for the refined SiRHP model*

The SiRHP model was refined with both *X-PLOR* and *TNT* against 1.6 Å resolution data (no σ cutoff applied) collected at 1.08 Å on SSRL beamline 7-1. R_{Test} was calculated against a test data set containing 10% of the reflections removed at random to approximate R_{Free} (Brünger, 1993). To avoid bias in the R_{Test} calculation because the test reflections were not removed before the model was completed, the coordinates were given normally distributed errors with an r.m.s. deviation of 0.22 Å before carrying out positional and thermal factor refinement until convergence. Adding errors to the coordinates increased the overall R factor in *X-PLOR* from 19.1% for the converged model to 26% for the partly randomized model. Interestingly, even if the coordinates were not randomized, R_{Test} relaxed to the same value against the released data. In keeping with the lower *TNT* R factor, stereochemical restraints were not as strict in the *TNT* refinement as in the *X-PLOR* refinement, although the r.m.s. bond and angle deviations still indicate good geometry. The bulk solvent correction in *TNT* allows inclusion and modeling of all low-resolution data and this also contributes to the lower R factor. The R factor calculated in *X-PLOR* for the *TNT*-refined model is 17.5% between 10.0 and 1.6 Å resolution. In both refinements, angle and bond restraints on the siroheme porphyrin ring and carboxylate side chains were the only stereochemical restraints applied to the cofactors. $R_{\text{merge}} = \sum_h \sum_i |I_{hi} - \langle I_h \rangle| / \sum_h \sum_i |I_{hi}|$.

Diffraction data						
Resolution (Å)	∞-3.57	3.57-2.53	2.53-2.06	2.06-1.79	1.79-1.60	∞-1.60
Observations (No.)	32748	61579	78617	91939	100080	364963
Unique reflections (No.)	5755	10338	13084	15257	16827	61261
Completeness (%)	96.4	98.6	98.0	97.2	93.3	97.0
R_{merge} (%)	8.5	8.5	10.0	14.1	24.1	9.9
Refined model	*X-PLOR*	*TNT*				
Total non-H scatterers	4186	4186				
Water molecules	486	486				
R.m.s.d. bond length (Å)	0.010	0.017				
R.m.s.d. bond angle (°)	1.6	2.5				
σ_A estimated r.m.s. coordinate error	0.18	0.17				
X-PLOR						
Resolution shells (Å)		10.0-2.50	2.50-2.00	2.00-1.76	1.76-1.60	10.0-1.60
Overall completeness (%)		98.1	98.0	97.0	93.5	96.7
R factor (%)		16.6	19.0	22.5	27.8	19.1
R_{Test} (%)		20.5	20.9	23.9	27.6	21.8
TNT						
Resolution shells (Å)		∞-2.50	2.50-2.00	2.00-1.76	1.76-1.60	∞-1.60
R factor (%)		14.0	18.0	22.0	26.0	16.9
R_{Test} (%)		21.0	22.0	26.0	28.0	22.4

fall in bin $z = 1$ and all values greater than $(-w \cdot \sigma_M/2) + w \cdot \sigma_M \cdot$nbin fall into bin $z =$ nbin. These range limits are imposed on defining the histogram so that especially large or small electron-density values in a given map (resulting from, say, a metal atom) will not offset the histogram relative to maps derived from another protein. The relatedness of two histograms (M and N) can then be evaluated by a correlation function (R_H),

$$R_H = \frac{\sum_z f_z^M f_z^N - \sum_z f_z^M \sum_z f_z^N}{\left\{\left[\sum_z (f_z^M)^2 - \left(\sum_z f_z^M\right)^2\right]\left[\sum_z (f_z^N)^2 - \left(\sum_z f_z^N\right)^2\right]\right\}^{1/2}}. \quad (50)$$

A systematic search of experimental phase weights is then used to optimize R_H between a combined experimental map and a reference electron-density map calculated from a solved protein structure with similar solvent content.

3. Results and discussion

3.1. *Standard for assessment of improved phasing - the refined SiRHP model*

The methodology presented above, as implemented in the program *MADPHSREF*, ultimately resulted in a MAD-derived experimental electron-density map for SiRHP of higher quality than the MAD/MIR map originally used to determine the structure. In order to critically test these new procedures and guide the development of *MADPHSREF*, the refined SiRHP structure (Crane *et al.*, 1995) provided the necessary control. The SiRHP model has excellent stereochemistry and low R factors when refined both originally with *X-PLOR* (Brünger, Kuriyan & Karplus, 1987) and later with *TNT* (Tronrud, Ten Eyck & Matthews, 1987) against 1.6 Å resolution data collected at 1.08 Å on SSRL beamline 7-1 (Table 1). Prior to refinement with *TNT*, the *X-PLOR* converged coordinates were given Gaussian-distributed random errors that produced a root-mean-square (r.m.s.) deviation of 0.22 Å for all coordinates - a value slightly larger than the r.m.s. error estimated from a σ_A plot (Read, 1988). All experimental phase errors are calculated relative to structure factors derived from the *X-PLOR*-refined structure. The effectiveness of Fe-atom positional refinement against anomalous data was assessed by comparing the converged Fe-atom coordinates to the Fe-atom coordinates of the *X-PLOR*-refined structure, which are assumed to be 'true'.

Table 2. *Anomalous difference scattering vector amplitudes refined against simulated and experimental data sets*

For the generation of simulated data sets, anomalous-difference scattering amplitudes for iron and sulfur were taken from the *International Tables of X-ray Crystallography Vol.* IV (Ibers & Hamilton, 1974) and assigned as follows: $f''(\lambda_A) = f''$ at Cu $K\alpha$ (1.5418 Å), $f''(\lambda_B) = f''$ at Fe K (1.74 Å, an approximation for the K-edge value of 1.7412 Å). $\Delta f'(\lambda_{AB}) = \Delta f'(\lambda_{AC}) = f'(\lambda_{1.5418}) - f'(\lambda_{1.74})$. Refinement of difference scattering vector amplitudes against a simulated data set with no errors and fixed atomic positions (error-free simulation) reproduced the scattering factors used in generating the simulated data set (the starting values are in parentheses). SiRHP normal scattering vectors and the assigned anomalous-scattering vectors were combined to simulate 61 017 unique Bijvoet and dispersive differences. Refinement was run over the resolution range of 8.6–2.5 Å for 12 cycles to optimize the difference scattering vector amplitudes. Gaussian-distributed random errors were applied to the calculated structure-factor amplitudes in resolution shells of ∞–5.0, 5.0–3.5, 3.5–3.0, 3.0–2.7, 2.7–2.5 Å to give r.m.s.$(\Delta F/F)$ of 2.0, 2.5, 3.4, 5.2 and 8.0%, respectively (simulation with Gaussian errors). The magnitudes of f' and f'' used to calculate the starting difference vectors were obtained by X-ray absorption spectroscopy with the assumptions of isotropic anomalous scattering and anomalous scattering from iron alone (Crane *et al.*, 1997). To generate the experimental difference vector magnitudes, relative Wilson scaling was used to put the MAD amplitudes on a quasi-absolute scale. Dispersive differences were taken only between reflections that had both Bijvoet pairs at each wavelength so that a reasonable estimate of $|\overline{F}|$ could be made $\{\sigma\Delta|F^{\pm}(\lambda_i)| = [\sigma\Delta|F^{+}(\lambda_i)|^2 + \sigma\Delta|F\ (\lambda_i)|^2]^{1/2},\ \sigma\Delta|\overline{F}(\lambda_{ij})| = [\sigma\Delta|F^{\pm}(\lambda_i)|^2 + \sigma\Delta|F^{\pm}(\lambda_j)|^2]^{1/2}\}$. In addition to iron spatial parameters, individual scale and thermal factors for nine crystal positions were refined simultaneously for 12 cycles using a rejection level of 0.8 for Ze to reject 8617/41 135 reflections on the last refinement cycle. Initial Fe-atom positions had an r.m.s. deviation of 0.66 Å from their final refined values in the 1.6 Å resolution SiRHP model, and S-atom positions were held at their true values. Atomic positions, scale and thermal factors were then fixed and scattering factors were refined for ten cycles.

	Assigned		Error-free simulation		Simulation with Gaussian errors		SiRHP refined	
	Fe	S	Fe	S	Fe	S	Fe	S
$f''(\lambda_A)$	3.09	0.557	3.35 (4.0)	0.56 (0.4)	2.04 (4.0)	0.85 (0.4)	3.48 (3.14)	0.35 (0.0)
$f''(\lambda_B)$	4.98	0.847	5.30 (4.0)	0.83 (0.4)	6.13 (4.0)	0.48 (0.4)	4.40 (4.73)	0.37 (0.0)
$\Delta f'(\lambda_{AB})$	4.72	−0.510	4.56 (7.0)	−0.01 (0.1)	4.30 (7.0)	−0.04 (0.1)	5.55 (4.72)	−0.09 (0.0)
$\Delta f'(\lambda_{AC})$	7.19	−0.510	6.95 (7.0)	0.00 (0.1)	7.75 (7.0)	−0.06 (0.1)	7.69 (7.08)	−0.01 (0.0)

3.2. *Assessment of the refinement procedure and its ability to incorporate multiple types of anomalous scatterers*

Simulated data sets were generated to test if the MAD phase-refinement procedure, as implemented in *MADPHSREF* and presented above, could reproduce accurate phases, successfully refine native Fe-atom positions and detect S-atom anomalous scattering from native SiRHP. In addition to five Fe atoms, SiRHP has 20 ordered S atoms in the final refined structure (four-cluster inorganic S atoms, six cysteine thiolates and ten methionines) that each make a small contribution to the anomalous scattering model at the Fe K and Cu $K\alpha$ energies. For the simulated and experimental data sets, two Bijvoet differences $[\Delta|F^{\pm}(\lambda_A)|$ and $\Delta|F^{\pm}(\lambda_B)|]$ and two dispersive differences $[\Delta|\overline{F}(\lambda_{AB})|$ and $\Delta|\overline{F}(\lambda_{AC})|]$ were generated from the refined SiRHP coordinates and *a priori* anomalous scattering vectors (Table 2). The remaining two possible difference terms that have the smallest intrinsic magnitudes, $\Delta|F^{\pm}(\lambda_C)|$ and $\Delta|\overline{F}(\lambda_{BC})|$, did not improve phase estimates for the experimental data when included, and therefore were ignored for most calculations. Refinement against real and simulated data was carried out by estimating phases, root-mean-square (r.m.s.) errors, correlation coefficients and figures-of-merit (FOM's) between cycles of optimizing individual atomic parameters (positional and thermal), local scale and local thermal parameters, and anomalous difference vector magnitudes. Local overall scale and thermal parameters were optimized for separate wedges of diffraction data containing reflections collected closely together in time and reciprocal space.

The magnitudes of the anomalous difference scattering vectors $[f''(\lambda_i), \Delta f'(\lambda_{ij})]$ reproduced values derived from experimental measurements of f'' and $\Delta f'$ for both iron and sulfur when refined against error-free simulated data, even if the initial scattering vector magnitudes did not distinguish the real relative magnitudes (Table 2). In contrast, when resolution-dependent errors comparable to those found in the SiRHP experimental observations were added to the amplitudes, the relative magnitudes of the small sulfur vectors no longer refined correctly. Large errors in both the atomic anomalous difference scattering factors and the atomic positions prevent accurate refinement of both sets of parameters simultaneously. For example, if a simulated data set is generated where one of the iron–sulfur cluster Fe atoms is substituted by cobalt and the atoms are given a 0.7 Å r.m.s. positional error, the cobalt scattering factors will not refine accurately from initial values set for iron. However, if estimates of the atomic difference scattering factors are known experimentally, then both scattering factors and atomic positions can be simultaneously optimized. Even though SiRHP's isotropic f'' and f' values were determined using X-ray fluorescence measurements under the assumption of only anomalously scattering iron, the sulfur difference scattering factors, initially set to zero, refined to reasonable values and the starting iron values adjusted appropriately (Table 2).

The loss of almost all phase and positional error after the refinement of incorrect Fe-atom positions (r.m.s. deviation = 0.66 Å from the 'true' coordinates) against

Table 3. *Errors introduced by excluding sulfur anomalous scattering*

The anomalous-difference phase-refinement protocol was tested by refining an anomalous scattering model for SiRHP against error-free simulated data (see legend to Table 2) both when the model included (5Fe-20S) and excluded (5Fe) SiRHP native sulfur anomalous scattering. Inclusion of sulfur anomalous scattering resulted in significantly smaller, overall, amplitude-weighted, acentric phase errors $\sum |F| \Delta\varphi / \sum |F|$ ($w\langle\Delta\varphi\rangle_{over}$); smaller r.m.s. deviations in the converged Fe-atom positions from their 'true' values (ΔFe); and a higher electron-density map correlation coefficient (R_c), compared to the refined structure. $R_c = \langle\rho_e\rho_r\rangle - \langle\rho_e\rangle\langle\rho_r\rangle / [\langle\rho_e^2\rangle - \langle\rho_e\rangle^2]^{1/2}[\langle\rho_r^2\rangle - \langle\rho_r\rangle^2]^{1/2}$, where ρ_e is the electron density of the FOM-weighted experimental map, and ρ_r is the final $2F_o - F_c$ electron density phased with the refined structure. Starting Fe-atom coordinates had an r.m.s. deviation of 0.66 Å from their 'true' values and the S-atom spatial parameters were not refined. For SiRHP map correlation calculations, experimental phases and FOM's are combined with amplitudes essentially unperturbed by anomalous scattering from a 1.6 Å resolution native SiRHP data set collected at a wavelength of 1.08 Å (Crane *et al.*, 1995).

	Error-free simulation		Simulation with Gaussian errors		SiRHP	
	5Fe-20S	5Fe	5Fe-20S	5Fe	5Fe-20S	5Fe
$w\langle\Delta\varphi\rangle_{over}$ (°)	7.2	12.5	47.8	48.6	59.0	59.0
R_c	0.946	0.917	0.536	0.531	0.458	0.458
ΔFe (Å)	0.021	0.043	0.079	0.129	0.275	0.279

error-free simulated data demonstrates that although (12) and (19) contain approximations they are appropriate target functions (Table 3). Even in the presence of substantial simulated errors the inclusion of sulfur anomalous scattering reduced phase errors and deviations from ideal iron geometry, and also increased the map correlation coefficient (R_c) calculated between an $|^{\circ}F_T| \times$ FOM experimental map and the $2F_o - F_c$ map of the refined structure (Table 3). However, the errors in the SiRHP experimental data were large enough that sulfur anomalous scattering was barely significant and, therefore, it is reasonable to neglect the S atoms for refinement against this data. The phase errors determined for the SiRHP experimental data are larger than those resulting from refinement against simulated data with Gaussian errors (Table 2), which implies that either errors on the real $|F|$'s are larger than those simulated, or that the experimental errors are not Gaussian in nature. Given that the simulated data have r.m.s. errors on $|F|$ of 5.2–8.0% in the highest resolution bins (legend to Table 2), and that the errors in the observed SiRHP data are higher than this, it seems remarkable that the relatively small SiRHP anomalous signals provide phase restraints sufficient for structure determination.

3.3. *Refinement of thermal parameters*

Anomalous scattering is less sensitive than normal scattering to attenuation with increased scattering angle because the electronic transitions involved occur from tightly bound orbitals that have much smaller radii than the valence orbitals that dominate normal scattering. Accordingly, the exponential terms used to model the attenuation of scattering intensity with increased angle in normal scattering factors are not included in the difference anomalous scattering factors ($\Delta f_q'$ and f_q''). Intensity fall-off with increased scattering angle as a result of thermal disorder will also be less for anomalous scattering than for normal scattering because the convolution of the orbital expanse with the mean-square atomic displacement is generally smaller for electrons contributing to anomalous scattering than for electrons contributing to normal scattering (Helliwell, 1992). Consequently, if the individual exponential thermal factors associated with each atom are fixed at the individual B values found from the normal scattering refinement, the thermal factors that model overall scattering attenuation with increased scattering angle for a local set of reflections refine to negative values. Because the relative motion of the atoms, reflected in the individual thermal parameters, are the same for anomalous and normal scattering, the local thermal parameters that apply to all reflections of a given orientation should account for (i) decreased sensitivity of the anomalous signal to increased resolution, (ii) increased diffraction decay resulting from crystal radiation damage for the MAD data relative to the native data, and (iii) measurement errors that likely increasingly over-represent large aberrant anomalous differences with higher resolution. Individual anomalous thermal parameters for each atom refined stably only when bivariate normal distributions were used to compensate for the correlations between residual errors in the lack-of-closure expressions [(30) and (31)]. Without compensation for correlations, the individual thermal parameters became unrealistically large and the refinement diverged. In the anomalous refinement, local and individual thermal parameters could not be refined together; thus, local thermal, local occupancy and positional parameters were refined first followed by individual thermal and positional parameters.

3.4. *Refinement weights*

Weighting the individual observations by FOM$\times 1/\sigma^2$ (where σ is the measured observation error in terms of counting statistics and background, and FOM is calculated from the previous phasing cycle) resulted in better convergence and more accurate Fe-atom positions than weighting by $1/(\sigma^2 + E^2)$, where E^2 is $\langle E_{ii}\rangle$ averaged over a range of reflections [see (36)]. Reflection partitions based on resolution, difference magnitude, and observation magnitude were attempted separately or in combination for averaging E^2 values. None of these strategies was as successful as the FOM weighting scheme. Because the normal scattering phase (φ_P) is

fixed in value during least-squares refinement, it is appropriate to weight the least-squares terms relative to each other by FOM, a factor that reflects the accuracy of φ_P at the current iteration. Although the $\langle E_{ii} \rangle$ values represent the width of the probability distribution for all parameters, their likelihood is only integrated over the parameter φ_P, and not the complex plane of the anomalous difference structure factors. Thus, the $\langle E_{ii} \rangle$ values include errors in parameters other than φ_P and, therefore, may not be as sensitive as FOM to the relative errors in φ_P from different reflections. Provided that there are reasonable estimates for the unaveraged parameters, weighting an individual term by a factor representative of that term's phase error, appears more effective than weighting by an overall closure error averaged over a large group of reflections.

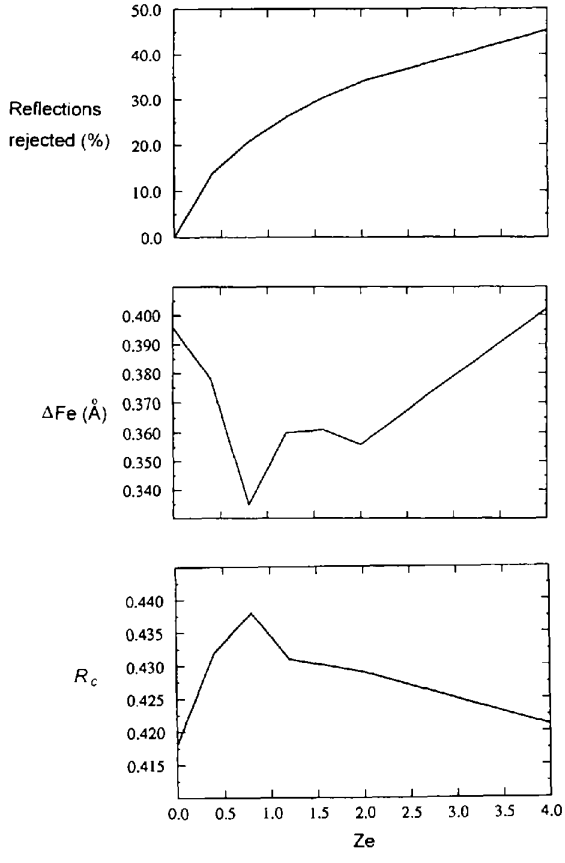

Fig. 2. Sensitivity of refinement to outlier rejection. The effect of rejections selected by increasing values of Ze on the r.m.s. deviation of Fe-atom positions from ideality (ΔFe) and the map correlation coefficient (R_c) at refinement convergence. Local scale, thermal parameters and Fe-atom positions were optimized over eight cycles of refinement against the experimental SiRHP data (41 135 total observations) without including S atoms in the model or applying any other rejection criterion (*i.e.*, σ cutoffs or cutoffs on large differences). A minimum in ΔFe correlates to a maximum in R_c when ~20% of the observations were rejected. At each cycle, all observations were allowed to contribute to the phase distributions, but the rejected reflections were excluded from refinement of the anomalous scattering model in that cycle.

3.5. *The rejection of outlying observations*

The probabilistic rejection of outlying measurements expressed by (44) and (45) was quite effective at mitigating the effects of bad measurements on refinement, while preventing the introduction of bias towards the starting model (Fig. 2). As the exponential multiplicative term that sets the rejection level (Ze) was increased from zero, the r.m.s. deviations in Fe-atom positions after eight refinement cycles decreased to 0.335 Å when 20% of the observations were rejected (8617/41 135 at Ze = 0.8). The map correlation coefficient (R_c), a reflection of the quality of experimental electron density (see legend to Table 3), is anticorrelated to ΔFe and reaches a peak value of 0.438 at Ze = 0.8 after eight cycles. Refinements carried out with cutoffs applied to the observation σ's and difference magnitudes to remove ~20% of the observations [8478 out of 41 135 reflections being rejected if $\Delta_{A \text{ or } D} \leq 0.55 \times \sigma\Delta_{A \text{ or } D}$ or $5.0 \times \text{r.m.s.}(\Delta_{A \text{ or } D}) \geq \Delta_{A \text{ or } D}$] do not minimize as effectively (ΔFe = 0.393 Å, R_c = 0.429) compared with the probabilistic selection procedure. Refinement against simulated data with Gaussian errors is also most successful when ~20% of the observations are excluded by the Ze term, indicating that even with normally distributed errors it is beneficial to remove the most aberrant observations.

Probabilistic sampling, as opposed to applying fixed cutoffs, allows all observed differences to be compared to continually improving calculated differences and error estimates. Since the residual errors are always compared to the current, most likely r.m.s. error estimates, more deviant observations will be tolerated when the anomalous scattering model is initially inaccurate. As the model begins to converge, the error estimates will start to reflect the true errors and the criteria for rejection will be more stringent. The random element of the probabilistic rejection method always allows observations that are not consistent with the current Fe-atom positions to still influence the refinement, and therefore reduces bias towards the current conformation. At early stages of refinement, it is difficult to assess if lack of closure stems from errors in the observations or errors in the anomalous scattering model. Instead of rejecting all inconsistent observations at the outset by some preset measure, the probabilistic approach considers both the likelihood of the model being correct and the likelihood of an

observation being consistent with that model at each progressive stage of refinement.

3.6. *Convergence of refinement and stereochemical restraints*

Refinement of an iron-only anomalous scattering model for SiRHP, having initial coordinates with an r.m.s. deviation of 0.655 Å from ideality, converges in approximately ten cycles of optimizing local scale, local thermal, and individual positional parameters followed by approximately ten cycles of optimizing individual positional, individual thermal and scattering-factor parameters when the experimental data is used (Fig. 3). ΔFe is well correlated with $\Delta\varphi$ and anti-correlated with R_c, demonstrating the importance of refining correct anomalous scatterer positions to calculating accurate phases. Stereochemical restraints on the interatomic Fe distances that force an idealized iron–sulfur cluster geometry decrease ΔFe on convergence, and this is also reflected in $\Delta\varphi$ and R_c (Table 4). Incorporating prior structural information on the metal centers, even relatively inaccurate distance restraints, can aid convergence to the correct conformation, especially with noisy data. FOM generally tracks $\Delta\varphi$ and R_c, but it is relatively insensitive to the addition of stereochemical restraints. The overall R factor between observed and calculated anomalous differences (Fig. 3) is a reasonable indicator for convergence, but its absolute value will always decrease with an increasing Ze (as

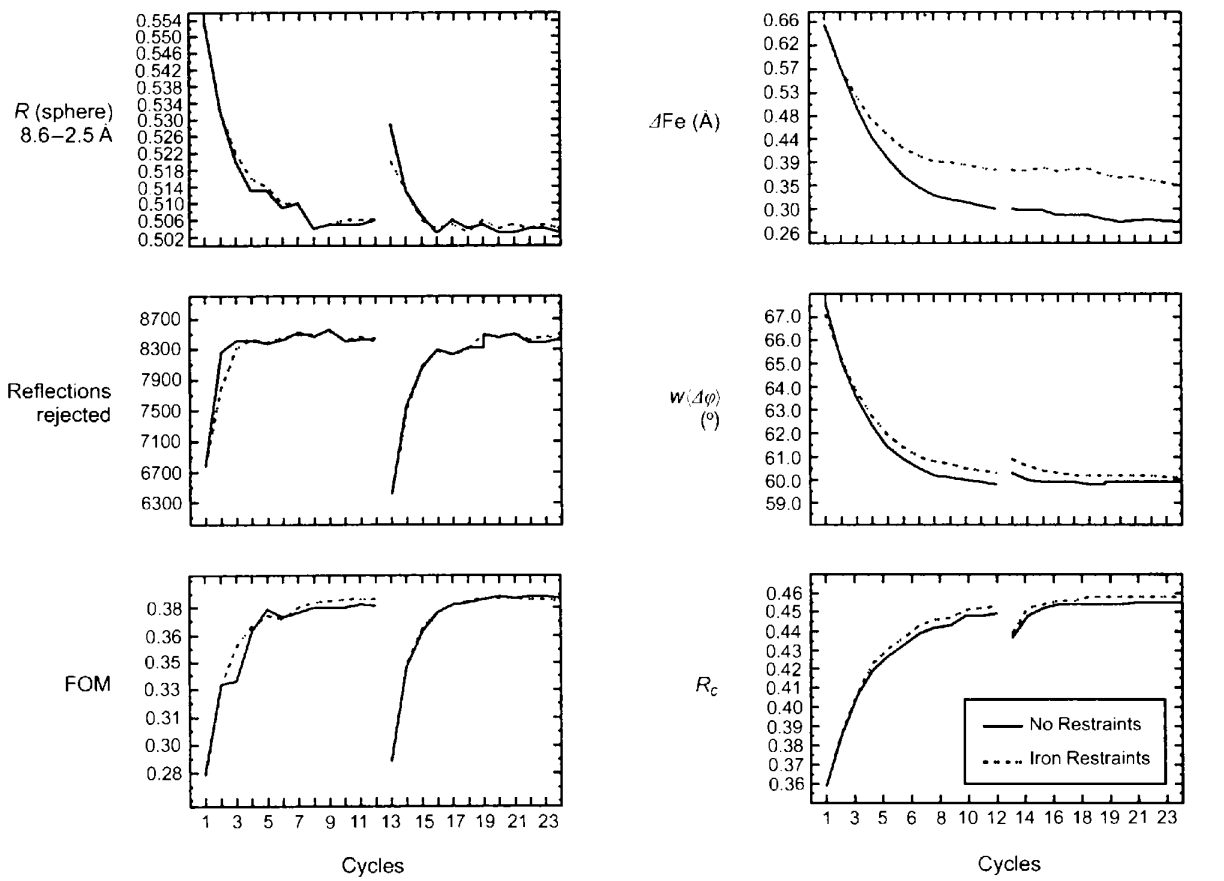

Fig. 3. Convergence of phase refinement and the effect of stereochemical restraints. Refinement statistics and parameters are monitored over 24 cycles of refinement. In the first 12 cycles, phases, positional parameters, and overall scale and thermal factors were concomitantly refined, and then positional parameters and individual thermal factors were refined for an additional 12 cycles. The discontinuity between these two sets of refinements results from re-evaluation of the likelihood error estimates and normal scattering phases at the start of the second stage. Starting Fe-atom coordinates had an r.m.s. deviation of 0.66 Å from their 'true' positions and Ze was set to 0.8 for outlier rejection. S atoms were not included in the model. Under stereochemical restraints (dotted line), all cluster Fe atoms were restrained to be 2.78 Å from each other, an average value for an idealized Fe_4S_4 cluster. The siroheme Fe atom was left unrestrained. Weights on the stereochemical terms were increased until 2.78 Å separations were achieved within the cluster by the last cycles of refinement. R(sphere) = $(\sum|\Delta_A| + \sum|\Delta_D|)/[\sum\Delta|F^{\pm}(\lambda_i)|_{obs} + \sum\Delta|\bar{F}(\lambda_{ij})|_{obs}]$ over the resolution range 8.6–2.5 Å. FOM = figure of merit [(35)]. ΔFe = r.m.s. deviation of Fe-atom positions from their 'true' positions at the end of refinement. $w\langle\Delta\varphi\rangle$ = overall amplitude weighted phase error, R_c = experimental map correlation to final $2F_o - F_c$ map calculated from 10.0–2.5 Å resolution (see the legend to Table 3).

Table 4. *More sophisticated error models and stereochemical restraints improved phase and scatterer refinement against anomalous differences*

Average phase errors ($\langle\Delta\varphi\rangle$) and overall weighted phase errors $w\langle\langle\Delta\varphi\rangle_{over}\rangle$ measured in °, and map correlation coefficients (R_c), calculated at the end of phase refinement, improved with an increasingly more complex error model. Local thermal, scale and Fe-atom positional parameters were refined over ten cycles with Ze = 0.8. S atoms were not included in the anomalous-scattering model. Overall completeness of unique reflections phased to 2.5 Å is 70%. The ability of the estimated FOM to represent $|\cos(\Delta\varphi)|$ is much improved when maximum likelihood estimates of r.m.s. errors are taken by averaging over all values of phase (+ likelihood error estimates), as opposed to being calculated at the centroid phase of the previous iteration (anomalous difference phase refinement). Additionally, compensating for correlations between Bijvoet difference residuals and dispersive difference residuals (+ correlation corrections) further improved phases and error estimates, and resulted in lower r.m.s. deviations from ideal Fe-atom coordinates on convergence (ΔFe). Internal stereochemical restraints on the Fe_4S_4 cluster (+ stereochemical restraints) aid convergence to ideal Fe-atom positions.

	Anomalous difference phase refinement		+ Likelihood error estimates		+ Correlation corrections		+ Stereochemical restraints	
Resolution (Å)	$\langle\Delta\varphi\rangle$	$\langle\lvert\cos\Delta\varphi$-FOM$\rvert\rangle$	$\langle\Delta\varphi\rangle$	$\langle\lvert\cos\Delta\varphi$-FOM$\rvert\rangle$	$\langle\Delta\varphi\rangle$	$\langle\lvert\cos\Delta\varphi$-FOM$\rvert\rangle$	$\langle\Delta\varphi\rangle$	$\langle\lvert\cos\Delta\varphi$-FOM$\rvert\rangle$
∞–6.0	45.7	0.15	43.7	0.10	43.6	0.09	43.4	0.07
6.0–4.3	50.4	0.20	48.6	0.10	46.8	0.01	46.9	0.00
4.3–3.5	67.9	0.35	66.5	0.10	64.8	−0.01	65.0	0.01
3.5–3.0	71.9	0.40	68.8	0.10	67.5	0.01	67.4	0.01
3.0–2.7	74.5	0.41	70.6	0.12	70.4	0.06	70.0	0.04
2.7–2.5	75.0	0.41	72.7	0.09	71.5	0.00	71.2	0.01
$w\langle\Delta\varphi\rangle_{over}$	63.5		60.7		59.3		59.0	
R_c	0.372		0.430		0.455		0.458	
ΔFe (Å)	0.464		0.415		0.345		0.279	

Table 5. *Improved phase errors and phase error estimates from MADPHSREF alone, and from the combination of MAD phases with MIR phases by histogram matching*

The *MADPHSREF* procedure resulted in much better phase errors and more accurate weights than the MAD-derived phases used in the original SiRHP structure solution (MAD_{comb}), where wavelength-independent parameters were calculated from (1) and then lack-of-closure expressions were used to generate probability distributions (Crane *et al.*, 1997). Overall completeness of unique reflections in the MAD_{comb} data set phased to 2.5 Å is 69%; however, only 51% of the unique reflections had at least four independent observations, the minimum number needed for direct phase determinations by *MADLSQ*. Compared with the original MAD_{comb}/MIRAS-weighted phase set, superior phases and more realistic FOM weights were obtained when *MADPHSREF*-derived phases were combined with MIRAS phases by using a weighting scheme determined by histogram matching electron-density distributions (*MADPHSREF*/$MIRAS_H$). Completeness of phased reflections in both combined data sets was nearly 100%.

	MAD_{comb}		*MADPHSREF*		MAD_{comb}/MIRAS		*MADPHSREF*/$MIRAS_H$	
Resolution (Å)	$\langle\Delta\varphi\rangle$	$\langle\lvert\cos\Delta\varphi$-FOM$\rvert\rangle$	$\langle\Delta\varphi\rangle$	$\langle\lvert\cos\Delta\varphi$-FOM$\rvert\rangle$	$\langle\Delta\varphi\rangle$	$\langle\lvert\cos\Delta\varphi$-FOM$\rvert\rangle$	$\langle\Delta\varphi\rangle$	$\langle\lvert\cos\Delta\varphi$-FOM$\rvert\rangle$
∞–6.0	48.4	0.22	43.4	0.07	42.9	0.20	40.3	0.24
6.0–4.3	50.2	0.21	46.9	0.00	45.4	0.19	41.7	0.04
4.3–3.5	71.1	0.34	65.0	0.01	64.4	0.34	59.5	0.01
3.5–3.0	74.8	0.37	67.4	0.01	68.9	0.32	65.2	0.01
3.0–2.7	78.6	0.36	70.0	0.04	77.4	0.39	73.3	0.12
2.7–2.5	80.7	0.32	71.2	0.01	84.2	0.44	78.4	0.17
$w\langle\Delta\varphi\rangle_{over}$	65.6		59.8		62.9		58.0	
R_c	0.340		0.443		0.430		0.486	
ΔFe (Å)	0.655		0.279		0.655		0.279	

Ze rejects observations inconsistent with the given model), and hence this statistic does not always reflect the best rejection strategy. Both the FOM and the number of reflections level at approximately four cycles as the likelihood error estimates stabilize.

3.7. *Error estimates and phase refinement*

Phase determination directly from the observed anomalous differences simultaneously optimizes anomalous scatterer positions and the phases derived from them. Compared with a least-squares treatment based on (1), which requires a fixed anomalous scatterer model (MAD_{comb}, Table 5), anomalous difference phase refinement utilizes more observations (a phase-probability distribution can be defined from a single pair of intensity observations), refines Fe-atom positions with more accuracy, and considerably reduces phase errors (Table 5). The FOM-weighted $|^{\circ}F_T|$ electron-density map calculated using the results from the difference refinement is generally less fragmented and has more regions of continuous 2σ density compared to the original MAD-phased map (Fig. 4). Previous attempts to define Fe-atom positions by refinement against $|^{\circ}F_A|$ values, or against Bijvoet differences at one wavelength [using the approximation that $|\sin(\psi_A - \varphi_P)| = 1$ for all large differences] were unsuccessful (Crane *et al.*, 1997). With the *MADPHSREF* procedure, incorporation of both Bijvoet and dispersive differences was necessary for stable

convergence with SiRHP experimental data. In addition to more accurate positional refinement and reduced phase errors, the difference refinement produced improved estimates of phase accuracy. Averaging error variances and covariances over all possible values of φ_P resulted in FOM's that better reflected the actual phase errors (Table 4). Accurate FOM's contributed to the generation of an improved experimental map by allowing the appropriate weighting of the Fourier terms (Fig. 4).

3.8. *Compensation for correlated errors*

Phase error was reduced, positional and thermal factor refinement was more stable, and phase weights were defined with greater accuracy when error correlations among Bijvoet terms and among dispersive terms were partially compensated for by employing bivariate normal distributions to represent the probability distributions of the observed differences [see (30) and (31)]. During the refinement of an anomalous scattering model, correlations will always exist between residual errors for anomalous differences of the same type [either $\Delta|F^{\pm}(\lambda_i)|$ or $\Delta|\overline{F}(\lambda_{ij})|$] because all calculated anomalous differences for the same reflection will be affected by the same errors in both the anomalous scattering model and the normal scattering model (*i.e.* the protein phase error, fixed in value for each cycle of refinement). This is especially true where one type of anomalous scatter dominates and hence only a scale

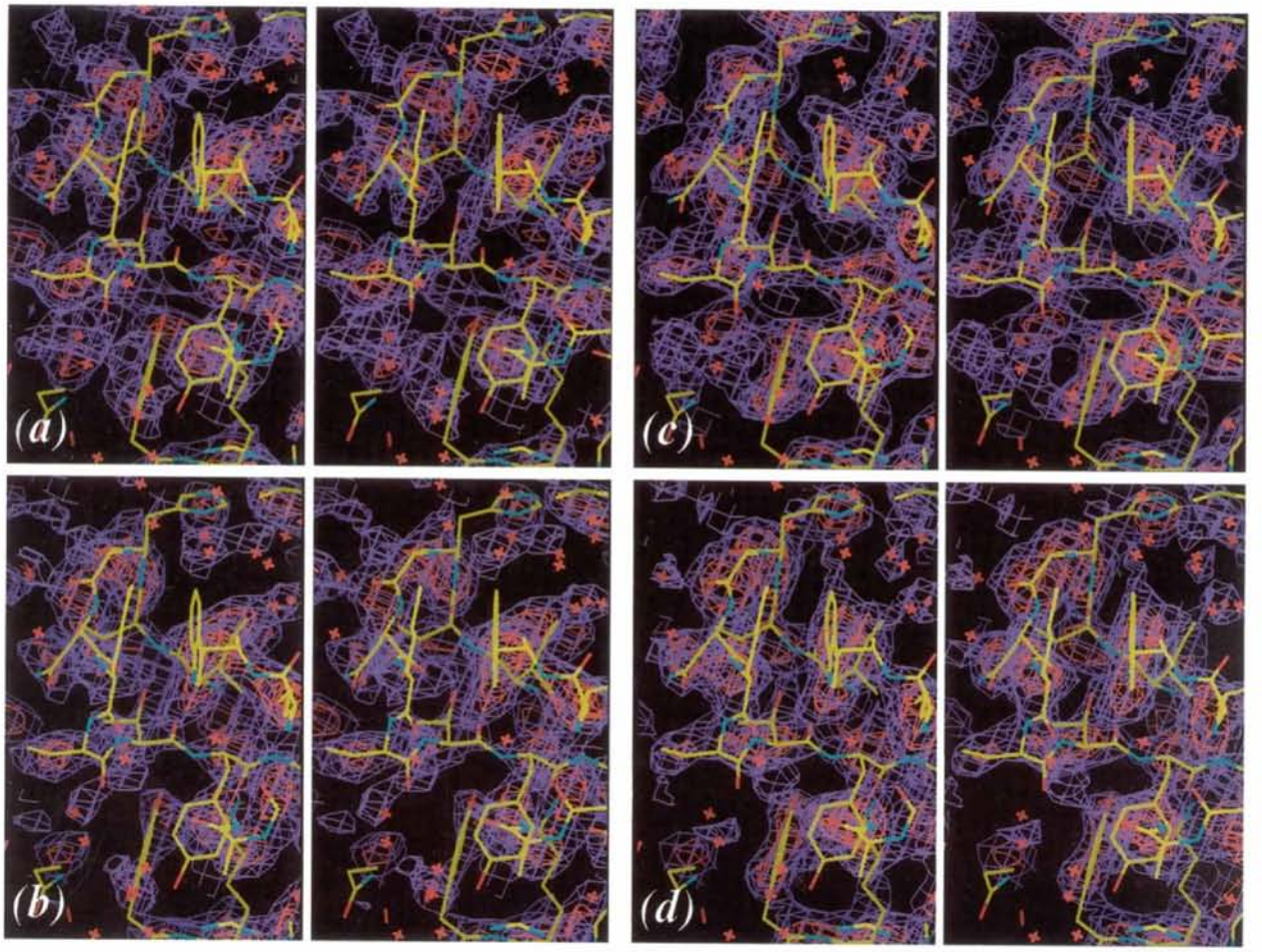

Fig. 4. Improvement in experimental electron-density maps. Anomalous difference refinement and improved error treatment results in better MAD electron-density maps and ultimately a superior MAD/MIR phase-combined map. (*a*) Stereoview of MAD_{comb} phased $|^{\circ}F_T|\times$FOM weighted, electron-density map (13.0–2.5 Å resolution, purple 1σ contours, red 2σ contours) showing an exposed loop between two β-strands in the SiRHP structure (see also Table 5). The map is fragmented, does not have many continuous regions at 2σ and does not conform well to the refined model (yellow C atoms, blue N atoms, red O atoms, water molecules shown as red crosses). (*b*) MAD_{comb}/MIRAS phased, $|^{\circ}F_T|\times$ FOM weighted, electron-density map (13.0–2.5 Å resolution) into which the original SiRHP model was built. (*c*) *MADPHSREF* phased, $|^{\circ}F_T|\times$ FOM weighted, electron-density map (13.0–2.5 Å resolution). This map is much improved from (*a*) and even more continuous than (*b*). (*d*) *MADPHSREF*/$MIRAS_H$ phased, $|^{\circ}F_T|\times$ FOM weighted, electron-density map (30.0–2.5 Å resolution). This map conforms more tightly to the model than (*c*), and the main-chain density is more continuous at the 2σ contour level, both here and in regions not shown. The figure was rendered with *XFIT* (McRee, 1992).

Table 6. *Correlation between the residual errors of anomalous differences*

Correlation coefficients between the residual errors of Bijvoet differences (Δ_A) and dispersive differences (Δ_D) taken at or between the three wavelengths of the experiment (A, B, and C) are given before (Initial) and after (Final) refinement of the anomalous scattering model and protein phases for simulated and SiRHP experimental data. Correlations were evaluated for SiRHP experimental data after Fe-atom positions, local scale, thermal parameters, FOM's and phases were refined over ten cycles with Ze = 0.8. S atoms were included in the calculations.

	Simulated data with Gaussian errors				SiRHP MAD data			
Resolution	$\Delta_A A/\Delta_A B$		$\Delta_D AC/\Delta_D AB$		$\Delta_A A/\Delta_A B$		$\Delta_D AC/\Delta_D AB$	
(Å)	Initial	Final	Initial	Final	Initial	Final	Initial	Final
∞–6.0	0.70	0.09	0.84	0.49	0.87	0.48	0.93	0.82
6.0–4.5	0.48	0.02	0.74	0.51	0.74	0.33	0.88	0.74
4.5–3.8	0.32	0.04	0.69	0.54	0.46	0.25	0.82	0.75
3.8–3.2	0.38	0.09	0.71	0.56	0.38	0.23	0.86	0.85
3.2–2.9	0.35	0.01	0.72	0.55	0.27	0.09	0.77	0.75
2.9–2.7	0.37	0.04	0.69	0.50	0.20	0.04	0.68	0.62

factor will relate different wavelength-dependent values of $F''_A(\lambda_i)$, and different wavelength-dependent values of $\Delta F'_A(\lambda_{ij})$. Another source of correlated error among dispersive differences arises because two or more differences will be taken relative to the same remote wavelength. Finally, for a MAD experiment where redundant measurements collected at different times, from different crystals, or from different regions of reciprocal space are not merged, observations measured from the same crystal orientation, through the same path-lengths and recorded in close spatial proximity on the detector face will be affected by the same experimental errors. The benefits of compensating for correlated error within a set of independent observations relating to an individual reflection are seen by larger values of R_c, the electron-density map correlation coefficient (Table 4). These improvements reflect not only reduced phase error, but also more appropriate FOM weights being applied to each reflection in the Fourier synthesis (Table 4). Refinement of individual thermal factors was stable only when the bivariate distributions were used and the refinement of these parameters does decrease the refinement residual and the phase error.

The mutual dependence of the anomalous differences on the Fe-atom positions and the normal scattering phase estimate caused complete correlation between the two Bijvoet difference error residuals and between the two dispersive difference error residuals when refinement was carried out against error-free simulated data. In contrast, there was no correlation between the residual errors from Bijvoet difference terms and from dispersive difference terms, justifying the strategy of separating the anomalous signal into Bijvoet and dispersive differences. When data with normally distributed amplitude errors were refined, initial correlations did exist between pairs of Bijvoet residuals and between pairs of dispersive residuals, but as convergence was reached and systematic errors in the protein phase and anomalous scattering model became small compared to the random amplitude errors, the correlations decreased to zero for the Bijvoet terms and 0.5 for the dispersive terms (the correlation of 0.5 arises from both dispersive differences being measured relative to the same remote wavelength) (Table 6). In the SiRHP experimental data, the anomalous and dispersive correlations are larger and did not reduce to their respective minimum values of 0.0 and 0.5 on convergence. This reflects either substantial errors remaining in the anomalous and normal scattering models used to calculate the anomalous differences, or additional correlations within the experimental data resulting from systematic measurement error for observations collected closely together in time and reciprocal space. Compensation for correlations in Bijvoet and dispersive residuals produced a faster and more accurate convergence when errors of the same direction were added to each simulated Bijvoet difference for a given reflection, but did not appreciably improve refinement against simulated data containing Gaussian errors without built-in correlations between terms.

3.9. *An empirical histogram-matching scheme for weighting MIR to MAD phases*

Empirical histogram matching of electron-density distributions is an effective scoring criterion for relative weighting of phases obtained from different sources. Reasonable estimates of MAD phase errors are provided by the difference refinement, but MIR phase errors can be grossly underestimated, and accordingly, their FOM's will be overestimated (Crane *et al.*, 1997). To compensate for such errors, the variances of the MIR probability distributions can be inflated by applying a multiplicative factor to their *ABCD* coefficients. Correlating electron-density histograms calculated from a combined MAD/MIR FOM-weighted map of SiRHP with a similar standard histogram calculated from a $2F_o - F_c$ map of a refined protein crystal structure with similar solvent content identified the most beneficial MIR phase weights relative to the MAD phases (Fig. 5). Resolution-dependent weights were then systematically applied to the MIR phases and each resultant combined phase set was scored against a suitable standard histogram to improve the weighting scheme. The correlation coefficient (R_H) between the SiRHP MAD/MIR combined map and the standard histogram reflected the average weighted phase error in the combined phase set quite well, despite only subtle contrast in R_H (Fig. 5). As expected, considerable down weighting of the MIR phases, especially at high resolution, resulted in the best histogram correlation

and a map that most closely mimicked the $2F_o - F_c$ map calculated from the refined structure. This final combined MIR/MAD map (*MADPHSREF*/MIRAS$_H$ Table 5, Fig. 4) is considerably improved over the original MIR/MAD map used to build the initial structure of SiRHP.

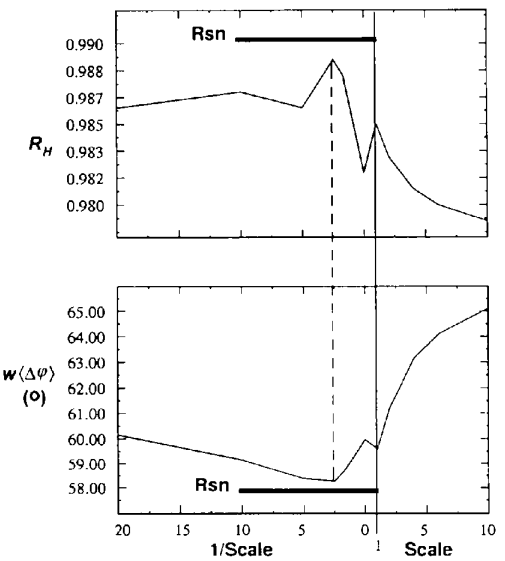

Fig. 5. Phase weighting by histogram matching. A single multiplicative scale factor (horizontal axis) was applied to the MIR Hendrickson-Lattman coefficients to increase or decrease the variance of the MIR phase distributions before addition to the MAD elicited coefficients. The weighting scheme was assessed by comparing correlation coefficients (R_H) between electron-density histograms calculated from the FOM-weighted phase-combined experimental map of SiRHP to a histogram generated from the $2F_o - F_c$ electron-density map of the uracil DNA-glycosylase (UDG) structure refined to 2.0 Å resolution (Mol *et al.*, 1995). The UDG crystals have an estimated solvent content of 38%, which is similar to the SiRHP value of 40%. The histograms were calculated in 100 evenly spaced bins between minimum and maximum electron-density values, which were defined as 6σ less or greater than the average electron-density value of 0.0 (F_{000} was not included in the Fourier synthesis). This relative choice for the minimum and maximum electron densities avoids offsetting the histograms by the presence of especially large or small density values in a particular structure, due, for instance, to metal ions. The weighted phase error ($w\langle\Delta\varphi\rangle$) reflects the correlation coefficient between the SiRHP and UDG histograms. There is discontinuity in the curve at 0 scale (no MIR contribution) because inclusion of MIR phases not only improved the histogram match by producing more accurate combined phases, but also by increasing overall completeness. Resolution-dependent MIR scale values further improved the weighting scheme. The data were broken into four equal divisions of $(\sin\theta/\lambda)^2$, and MIR scale factors were systematically searched starting with the lowest resolution bin and proceeding through the higher resolution bins. Scale factors giving the highest correlations were kept and applied to their respective resolution bins while the higher bins were searched. The final set of resolution-dependent scale factors (1.0 for 10.0–5.0 Å, 0.6 for 5.0–3.5 Å, 0.4 for 3.5–2.8 Å and 0.1 for 2.8–2.5 Å) reflected the MIR phase error (Crane *et al.*, 1997) and produced the combined map with the highest value of R_H and the lowest weighted phase error (represented by the horizontal black bar and labeled Rsn).

Table 7. *Refinement of Fe_4S_4 cluster asymmetry*

SiRHP Fe_4S_4 cluster asymmetries are compared for conjugate-gradient normal-scattering refinement in *X-PLOR* (Powell, 1977; Brünger *et al.*, 1987) (1.6 Å *X-PLOR*), conjugate-direction normal-scattering refinement in *TNT* (Tronrud, 1992) (1.6 Å *TNT*), and a full-matrix least-squares refinement of the Fe-atom positions against the anomalous and dispersive differences (2.5 Å AR). For the *X-PLOR* and *TNT* refinements, distances are shown for two different starting conformations where the coordinates of the entire model were given Gaussian-distributed random errors with an r.m.s. deviation of 0.22 Å. In the normal-scattering refinements, atomic scattering factors for Fe atoms in the iron–sulfur cluster were set to the average of the values for Fe^{2+} and Fe^{3+} to reflect the formal charge of +2.5 on the SiRHP Fe_4S_4 cluster irons. However, changing the Fe-atom scattering factors to represent either Fe^{2+} or Fe^{3+} does not affect the converged cluster coordinates. For the anomalous refinements, which were carried out using data between 8.5 and 2.5 Å resolution, the average converged iron separations are given for 12 different random starting conformations (with an r.m.s. deviation of 0.65 Å).

Fe_4S_4	1.6 Å *X-PLOR*		1.6 Å *TNT*		2.5 Å AR
Distance (Å)					
Fe1—Fe2	2.80	2.80	2.75	2.74	2.68
Fe1—Fe3	2.80	2.79	2.77	2.76	2.84
Fe1—Fe4	2.70	2.70	2.66	2.67	2.67
Fe2—Fe3	2.79	2.76	2.72	2.72	2.75
Fe2—Fe4	2.77	2.76	2.75	2.73	2.73
Fe3—Fe4	2.81	2.80	2.76	2.76	2.79
HFe—Fe4	4.48	4.48	4.51	4.51	4.44

3.10. *The assessment of subtle asymmetries in the SiRHP Fe_4S_4 cluster*

Three refinement procedures were applied for defining the geometry of the Fe_4S_4 cluster in SiRHP. Powell conjugate-gradient normal-scattering refinement of SiRHP in *X-PLOR* (Powell, 1977; Brünger *et al.*, 1987) against 1.6 Å resolution synchrotron data, with the Fe_4S_4 cluster, cysteine thiolate ligands, and siroheme iron unrestrained (Crane *et al.*, 1995), identified a subtle asymmetry in the Fe_4S_4 cluster cubane. At least one Fe—Fe distance (Fe1—Fe4), involving the cubane iron bound to the siroheme-bridging thiolate ligand, is significantly shorter than the others (Table 7). Normal-scattering refinement of SiRHP with conjugate-direction minimization as implemented in *TNT* (Tronrud *et al.*, 1987; Tronrud, 1992) also identified the Fe1—Fe4 distance as being shortest, although all of the distances were somewhat smaller compared with the *X-PLOR* refinement (Table 7). Conjugate-direction minimization uses a diagonal approximation of the normal matrix to weight parameter shifts by curvature, and thereby prevents the over-shifting and oscillatory behavior of parameters with large curvatures. These parameters can include the positional parameters for atoms with a relatively large number of electrons, such as the Fe atoms of SiRHP. Refinement of the Fe-atom positions against the multi-wavelength Bijvoet and dispersive differences has the advantage of only being dependent on the parameters of the anomalously scattering atoms. Thus, the refinement

is much more overdetermined than a normal-scattering refinement and the normal matrix can be inverted to determine estimated standard deviations (e.s.d.) on individual parameters.

Refinement of the SiRHP Fe-atom positions was carried out against the multiwavelength anomalous differences with *MADPHSREF* by assuming a fixed value of φ_P calculated from the *X-PLOR* refined structure. Because there was considerable noise in the anomalous data, especially in the high-resolution shells, many differences did not carry the correct sign; hence, convergence could not be reached if all reflections were included. In the final cycle of the probabilistic rejection approach of (44) and (45) 8079/11 990 reflections were accepted in the range of 8.5–2.5 Å resolution. The refinement consistently produced a final residual R factor [see R(sphere) in legend to Fig. 3] of 0.458, independent of starting conformation. Refinement against Bijvoet differences from only one wavelength was unstable and did not converge to reasonable geometry. The e.s.d.'s calculated by *MADPHSREF* (see below) are a function of the goodness of fit, which directly represents the agreement between residuals and the accuracy of the model employed.

The anomalous difference refinement with *MADPHSREF* also verified the smaller Fe1—Fe4 separation, but suggested that a second separation, Fe1—Fe2, was as small (Table 7). The e.s.d. for one Fe—Fe separation in a single refinement was 0.04 Å; however, the e.s.d. determined from the distribution of 12 different converged coordinates sets, each refined from partly randomized starting conformations, was 0.01 Å, which indicates that the minimum is well defined. Thus, all three refinement protocols suggest that the shortest Fe—Fe separation in the SiRHP cluster is between Fe1 and Fe4, although there is some variation in the relative lengths of the other refined distances. With the exception of Fe1—Fe2 separation in the anomalous refinement, all other inter-iron distances are ~0.1 Å longer than the Fe1—Fe4 separation (Table 7). Such deviations of the SiRHP cluster from typical Fe_4S_4 cluster D_{4h} point symmetry, are consistent with resonance Raman spectroscopy (Madden, Han, Siegel & Spiro, 1989) and may have implications for electronic coupling to the siroheme. With high-resolution anomalous diffraction data, refinement against multiwavelength anomalous differences in this manner may help determine extremely accurate geometries for protein metal clusters in other systems.

4. Conclusions

For MAD data with large experimental errors and limited phasing restraints (such as were collected on SiRHP), calculating protein phases directly from the observed Bijvoet and dispersive differences appears more effective than determining wavelength-independent terms with the complete scattering equation. This latter approach is more rigorous and has proven very successful when the data are well measured, strong and redundant. However, the least-squares optimization of local parameters will suffer from indeterminacy if there are an insufficient number of measured observations per individual reflection and reasonable probability distributions are difficult to obtain when the phases are not well restrained. *MADPHSREF* uses all observations to optimize simultaneously a global anomalous scattering model from which local phases are calculated, as opposed to initially estimating local parameters for each reflection and then refining a global anomalous scattering model against these local parameters. The *MADPHSREF* approach requires as little as one pair of observations to define a probability distribution for a given reflection.

Phase refinement against anomalous differences has been applied successfully in the past. In a treatment analogous to phase determination by isomorphous replacement, the relationship expressed in (12) has been used to map dispersive differences back to a single wavelength and generate pseudo-native and pseudo-derivative data sets, while assuming ψ_D constant for all wavelengths (Terwilliger, 1994). However, with multiple types of anomalous scatterers present, ψ_D and ψ_A, as well as $|F''_A(\lambda_i)|$ and $|\Delta F'_A(\lambda_{ij})|$ become wavelength-dependent. This also implies that $\psi_A \neq \psi_D + \pi/2$. Thus, with multiple anomalous scatterers, it is preferable to obtain phase information directly from the observed Bijvoet and dispersive differences rather than map these differences back to a monochromatic model while assuming the anomalous phase invariant. The relationship of (19) has been used to refine anomalous scatterer positions for myohemerythrin (Sheriff & Hendrickson, 1987) and to phase completely the structure of crambin from the intrinsic anomalous scattering of its S atoms (Hendrickson & Teeter, 1981). However, for the refinement of the anomalous scatterer positions these analyses select only large Bijvoet differences and hence assume unit magnitude for the cosine of (19).

Despite its limitations the procedure of iteratively calculating phases between cycles of least-squares refinement, long applied to the determination of heavy-atom positions in MIR, is better suited for MAD data. This least-squares approach is not a true maximum-likelihood optimization, because φ_P (an implicit function of the refined parameters) is fixed during each cycle and the variances are continually updated. These approximations introduce biases that can result in over-estimated occupancies for dominant heavy atoms, although averaging variances over all phase values mitigates these effects (Otwinowski, 1991). This problem is diminished for native metal clusters of a MAD experiment where occupancies can usually be assumed to be one. However, thermal factors

for the anomalously scattering atoms reflect a resolution-dependent occupancy and thus they can be potentially underestimated. Crystal isomorphism inherent in a MAD experiment also simplifies the application of this method. Although correlations in error are potentially more pervasive in a MAD experiment compared to an MIR experiment, multivariate normal distributions are partially able to compensate, as demonstrated by the improvement in error estimation and convergence that these modifications yield with SiRHP experimental data.

The effectiveness of most *de novo* phasing procedures for macromolecules depends on the reconciliation of a well defined perturbative scattering model with pairs of observed amplitudes. Parameterizing anomalous scattering models for native protein metal clusters can be difficult, especially where multiple types of anomalous scatterers are coordinated in asymmetric geometries. *MADPHSREF* compensates for multiple types of anomalous scatterers and allows the incorporation of prior structural knowledge in the form of distance restraints on the anomalous scatterers. In the presence of large observational errors, the anomalous scattering from SiRHP's 20 S atoms did not appreciably invalidate the assumption of an anomalous scattering model containing only iron. However, if experimental errors are relatively small, or the ratio of S atoms to metal atoms were larger, S atoms contained in protein–metal clusters could make a significant anomalous scattering contribution, and accounting for this may be warranted. The SiRHP anomalous refinement demonstrates that geometrical restraints can considerably assist in convergence to the true conformation.

Finally, our results with SiRHP demonstrate that full-matrix least-squares refinement of the anomalous scatterer coordinates against high-resolution MAD data can generate potentially more accurate protein metal-center models. Additionally, this method provides error estimates for positional parameters that are generally unattainable from conventional protein crystallographic refinement. The ability to define accurately the geometry and coordination of metal ions in enzymes should help us further understand the influence of the protein moiety on these centers and ultimately how metallic cofactors and proteins couple to achieve catalysis and control electron transfer.

We thank H. Bellamy for help with MAD data collection, the Stanford Synchrotron Radiation Laboratory for the use of data collection facilities, L. F. Ten Eyck for advice on refinement and critical reading of the manuscript, J. A. Tainer for useful discussions and advice, and W. A. Hendrickson for support and supplying the *ANOSYS/MADSYS* software, which provided a starting point for the development of *MADPHSREF*. *MADPHSREF* and supporting programs are freely available from the authors (crane@scripps.edu and edg@scripps.edu). This work was supported by NIH grant GM37684 to EDG and an NSERC fellowship to BRC.

References

Blow, D. M. & Matthews, B. W. (1977). *Acta Cryst.* A**29**, 56–62.

Bricogne, G. (1984). *Methods and Applications in Crystallographic Computing*, edited by S. R. Hall & T. Ashida, pp. 141–151. Oxford: Clarendon Press.

Bricogne, G. (1991). *Crystallographic Computing 5 - From Chemistry to Biology*, edited by D. Moras, A. D. Podjarny & J. C. Thierry, Vol. 5, pp. 257–297. Oxford University Press.

Brünger, A. T. (1993). *Acta Cryst.* D**49**, 24–36.

Brünger, A. T., Kuriyan, J. & Karplus, M. (1987). *Science*, **235**, 458–460.

Crane, B. R., Bellamy, H. & Getzoff, E. D. (1997). *Acta Cryst.* D**52**, 8–22.

Crane, B. R., Siegel, L. M. & Getzoff, E. D. (1995). *Science*, **270**, 59–67.

Dickerson, R. E., Kendrew, J. C. & Strandberg, B. E. (1991). *Computing Methods and the Phase Problem in X-ray Crystal Analysis*, edited by R. Pepinsky, J. M. Robertson & J. C. Speakman, pp. 236–251. Oxford: Pergamon Press.

Dodson, E. J. (1976). *Crystallographic Computing Techniques*, edited by F. R. Ahmed, K. Huml & B. Sedlacek, pp. 259–268. Copenhagen: Munksgaard.

Helliwell, J. R. (1992). *Macromolecular Crystallography with Synchrotron Radiation*. Cambridge University Press.

Hendrickson, W. A. (1991). *Science*, **254**, 51–58.

Hendrickson, W. A. & Lattman, E. A. (1970). *Acta Cryst.* B**26**, 136–143.

Hendrickson, W. A., Smith, J. L., Phizackerley, R. P. & Merritt, E. A. (1988). *Proteins Struct. Funct. Genet.* **4**, 77–88.

Hendrickson, W. A. & Teeter, M. M. (1981). *Nature (London)*, **290**, 107–113.

Hubbard, S. R., Wei, L., Ellis, L. & Hendrickson, W. A. (1994). *Nature (London)*, **372**, 746–754.

Ibers, J. A. & Hamilton, W. C. (1974). *International Tables for X-ray Crystallography*, Vol. IV. Birmingham: Kynoch Press. (Present distributor Kluwer Academic Publishers, Dordrecht.)

Karle, J. (1989). *Phys. Today*, pp. 22–29.

McRee, D. E. (1992). *J. Mol. Graphics*, **10**, 44–46.

Madden, J. F., Han, S., Siegel, L. M. & Spiro, T. G. (1989). *Biochemistry*, **28**, 5471–5477.

Mol, C. D., Arvai, A. S., Slupphaug, G., Kavil, B., Alseth, I., Krokan, H. E. & Tainer, J. A. (1995). *Cell*, **80**, 869–878.

Murthy, H. M. K., Hendrickson, W. A., Orme-Johnson, W. H., Merritt, E. A. & Phizackerley, R. P. (1988). *J. Biol. Chem.* **263**, 18430–18436.

Otwinowski, Z. (1991). *Isomorphous Replacement and Anomalous Scattering*, edited by W. Wolf, P. R. Evans & A. G. W. Leslie, pp. 80–86. Warrington: Daresbury Laboratory.

Powell, M. J. D. (1977). *Math. Program.* **12**, 241–254.

Read, R. J. (1988). *Acta Cryst.* A**42**, 140–149.

Shapiro, L., Fannon, A. M., Kwong, P. D., Thompson, A., Lehmann, M. S., Grubel, G., Legrand, J. F., Als-Nielson, J., Colman, D. R. & Hendrickson, W. A. (1995). *Nature (London)*, **374**, 327–337.
Sheriff, S. & Hendrickson, W. A. (1987). *Acta Cryst.* B**43**, 209–212.
Sim, G. A. (1959). *Acta Cryst.* **12**, 813–815.
Smith, J. L., Zaluzec, E. J., Wery, J., Niu, L., Switzer, R. L., Zalkin, H. & Satow, Y. (1994). *Science*, **264**, 1427–1433.
Sygusch, J. (1977). *Acta Cryst.* A**33**, 512–518.
Terwilliger, T. C. (1994). *Acta Cryst.* D**50**, 17–23.
Terwilliger, T. C. & Eisenberg, D. (1987). *Acta Cryst.* A**43**, 6–13.
Tronrud, D. E. (1992). *Acta Cryst.* A**48**, 912–916.
Tronrud, D. E., Ten Eyck, L. F. & Matthews, B. W. (1987). *Acta Cryst.* A**43**, 489–501.
Wilson, A. J. C. (1949). *Acta Cryst.* **2**, 318–321.
Wu, H., Lustbader, J. W., Lin, Y., Canfield, R. E. & Hendrickson, W. A. (1994). *Structure*, **2**, 545–558.
Zehna, P. W. (1970). *Probability Distributions and Statistics*. Boston: Allyn and Bacon Inc.
Zhang, K. Y. J. & Main, P. (1990). *Acta Cryst.* A**46**, 41–46.